PAPER

Interdigital and Multi-Via Structures for Mushroom-Type Metasurface Reflectors

Taisei URAKAMI[†a)], ***Student Member***, **Tamami MARUYAMA**[††], ***Member***, **Shimpei NISHIYAMA**[†††], **Manato KUSAMIZU**[†††], ***Student Members***, **Akira ONO**[†††], ***and*** **Takahiro SHIOZAWA**[††††], ***Members***

SUMMARY The novel patch element shapes with the interdigital and multi-via structures for mushroom-type metasurface reflectors are proposed for controlling the reflection phases. The interdigital structure provides a wide reflection phase range by changing the depth of the interdigital fingers. In addition, the multi-via structure provides the higher positive reflection phases such as near +180°. The sufficient reflection phase range of 360° and the low polarization dependent properties could be confirmed by the electromagnetic field simulation. The metasurface reflector for the normal incident plane wave was designed. The desired reflection angles and sharp far field patterns of the reflected beams could be confirmed in the simulation results. The prototype reflectors for the experiments should be designed in the same way as the primary reflector design of the reflector antenna. Specifically, the reflector design method based on the ray tracing method using the incident wave phase was proposed for the prototype. The experimental radiation pattern for the reflector antenna composed of the transmitting antenna (TX) and the prototype metasurface reflector was similar to the simulated radiation pattern. The effectiveness of the proposed structures and their design methods could be confirmed by these simulation and experiment results.

key words: *metasurface, reflector, interdigital, multi-via, ray tracing, electromagnetic field simulation*

1. Introduction

Recently, for obtaining broader bandwidth and higher data rates, the higher frequency band tends to be used in larger capacity wireless communication, especially in the fifth generation (5G) mobile communication. Due to the strong straightness propagation and the high path loss characters of the higher frequency wave, the signal coverage is severely limited especially for the non-line-of-sight (NLOS) regions [1]. The metallic passive reflectors, placed on the roof of the buildings etc., could be used as one of the solutions to this problem [2], [3]. Since the metallic reflectors reflect radio waves specularly, the reflection directions are limited.

For obtaining the preferable reflection directions, various reflectarrays [4]–[11] and metasurface reflectors [12]–[22] have been proposed. In most of reflectarrays, the reflection phase distributions are designed by changing their structural parameters of the elements on the wavelength scale, to obtain the desired reflection directions [4]. In [5]–[7], the reflectarrays with the half-wavelength crossed-dipole and loop-type frequency selective surface (FSS) were reported to obtain the dual polarization and multi-frequency operations. The reflectarrays based on the interdigital gap structures were proposed to realize a wide reflection phase range [8], [9]. For obtaining the smooth reflection phase gradient, the reflectarray with the I-shaped dipole element was reported [10]. The polarization conversion reflectarray with the double omega-shaped resonant elements, optimized by the genetic algorithm (GA) was also proposed [11]. On the other hands, the metasurface reflectors, of which reflection phase are designed by changing the *LC* resonant frequency, namely changing the loop inductance *L* and gap capacitance *C* of its smaller elements than the wavelength, were also proposed [12], [13]. In [14], [15], the multi-layer mushroom-type metasurface reflector were proposed to achieve a wide reflection angle. The H-type mushroom-type metasurface was also proposed to realize the multi-band reflector [16]. In [17], the beam switching method using the diode mounted metasurface was reported. The double layered patch-type FSS was also reported to achieve the variable reflection angle [18]. In [19], the multi-sheet configuration metasurface was reported to realize the broad beam width. The beam direction control, configured using the dipole antenna and its close placed metasurface, was proposed [20]. In [21], curved-type metasurface absorber which is thin was proposed to reduce the radar cross section (RCS). The low-profile and decoupling dipole antenna array using the metasurface with the C-shaped parasitic elements was also proposed [22].

The existing reflectarrays and metasurface reflectors, including the previous mentioned ones, could provide the various benefits for the 5G mobile communication systems. However, there would remain rooms to improve in these reflectors. The restrictions and design method for these reflectors would be discussed as follows.

In most of reflectarrays, their element sizes and spacing should be almost the same as its wavelength. However, reflectarrays that reflect at a wide angle require narrow element spacing compared with its wavelength. For this reason, designing reflectarray with wide angle reflection is difficult. Moreover, the mutual interaction between each element influences the reflection phase, therefore a flexible design considering element interference would be required to reduce

Manuscript received August 6, 2023.
Manuscript publicized January 15, 2024.

[†]The author is with Nara Institute of Science and Technology, Ikoma-shi, 630-0192 Japan.
[††]The author is with National Institute of Technology (KOSEN), Hakodate College, Hakodate-shi, 042-8501 Japan.
[†††]The authors are with National Institute of Technology (KOSEN), Kagawa College, Mitoyo-shi, 769-1192 Japan.
[††††]The author is with Toyo University, Kawagoe-shi, 350-8585 Japan.
a) E-mail: urakami.taisei.uo1@is.naist.jp

DOI: 10.23919/transcom.2023EBP3131

the degradation of the reflection characteristics. In the metasurface reflectors, a wide reflection angle can be achieved, since the size of elements is much smaller than its wavelength. However, in the conventional mushroom-type metasurface, the changeable elements sizes also become much smaller than its wavelength, therefore it is difficult to obtain the reflection phase range of ±180° at the design frequency, which are required to design the reflector. Especially, it is difficult to obtain the higher positive reflection phases such as near +180° and the lower negative reflection phases such as near −180° [12], [13]. For obtaining the reflection phases near −180°, several metasurfaces were proposed to increase the gap capacitance C [14]–[17]. On the other hands, the reflection phases near +180° could be obtained by decreasing the loop inductance L or gap capacitance C according to the normal incidence LC resonant theory [23], [24]. In [15], these reflection phases could be achieved by changing the thickness of the substrate for each patch to decrease the loop inductance L in the electromagnetic simulation, but it is difficult to realize these structures. In addition, in the conventional metasurface, it is difficult to place its patch elements closely and densely on the reflection plane, because its element size should be changed to obtain the desired reflection phases. These difficulties would cause the restrictions in the design and the deterioration of the reflection properties. By the way, in the case that the incident wave cannot be regarded as a plane wave, the Pozar's method [4] are commonly used for the reflector design. In the conventional Pozar's method, the path length from the phase center of the incident wave source to the reflection plane is required to obtain the incident wave phase distribution. However, it is difficult to define the accurate phase center of the wave source in some cases, for example in the near-field range of the transmitting antenna (TX). This is one of the difficulties of the conventional Pozar's method.

In this paper, the novel patch element shapes with the interdigital and multi-via structures for hexagonal mushroom-type metasurface reflectors are proposed to obtain the reflection phase range of ±180°. The interdigital structure provides a wide reflection phase range by changing the depth of the interdigital fingers. In addition, the multi-via structure provides the reflection phases near +180° by changing the distance from the patch center to the vias and the number of vias. Although the metamaterials including the interdigital structures appear in some literatures [25]–[30], introducing the interdigital structure to the metasurface with the hexagonal mushroom-type patches is the first attempt, to the best of the author's knowledge. The metasurfaces including the multi-via structures appear in some papers [31]–[35]. However, in most papers [31]–[33], the reflection phase properties were not remarked. For obtaining the reflection phases near +180°, introducing the multi-via structures to the metasurface is the first attempt, to the best of the author's knowledge. In these proposed structures, the patch elements could be placed closely and densely on the reflection plane, since the proposed structures could be composed of the common size hexagonal patch elements. Thus, these structures can be expected to improve the design freedom. These proposed structures could be also realized inexpensively using the usual double-sided print circuit board fabrication. Since the structural parameter number of the proposed hexagonal element shapes are more than that of the conventional square shapes, the proposed structures might have the property of controllability in the multi-dimensions.

In [36], we have already confirmed that the proposed reflector can control the direction of reflected waves in the case of the incident plane wave, using electromagnetic simulations. In this paper, the design method based on the ray tracing method using the incident wave phase is proposed, for applying the proposed structure to the arbitrary incident wave. Since the incident wave phase distribution could be obtained easily and accurately by electromagnetic simulation, the proposed design method is expected to provide the desired reflected phase distribution of the reflector, especially in the case of the arbitrary incident wave. In addition, the reflector antenna composed of the TX and the prototype reflector and its experimental results are shown with the simulation results, to confirm the potentiality of the proposed structure.

The remainder of this paper is organized as follows. In the Sect. 2, the proposed two structures are described and the reflection phases of these structures are simulated. The design method and the simulation results of the metasurface reflector for the normal incident plane wave are described in the Sect. 3. In the Sect. 4, the proposed design method using the incident wave phase distribution for the evaluation experiments are described. In the Sect. 5, the prototype reflector and its experimental results are described with the simulation results. The simulation results in this paper are obtained using the general-purpose electromagnetic field simulator Ansoft HFSS.

2. Interdigital and Multi-Via Structures

In this section, the novel patch element shapes with the interdigital and multi-via structures for mushroom-type metasurface reflectors are described. The interdigital structure provides a wide reflection phase range by changing the depth of the interdigital fingers. The multi-via structure provides the reflection phases near +180° by changing the distance from the patch center to the vias and the number of vias. Although the frequency bands of 28 GHz and 39 GHz are used in the 5G mobile communication of millimeter wave (mmWave), the design frequency f_0 of 6 GHz which will be used for 5G communication of sub-6 GHz band is chosen for matching to our next stage experimental setup. The application for the mmWave would be a future study.

2.1 Interdigital Structure Metasurface

Figure 1(a) shows the patch element shape with the interdigital structure. The interdigital structures are placed between adjacent patches. The hexagonal patches are connected to the ground plane on the back through vias represented by the

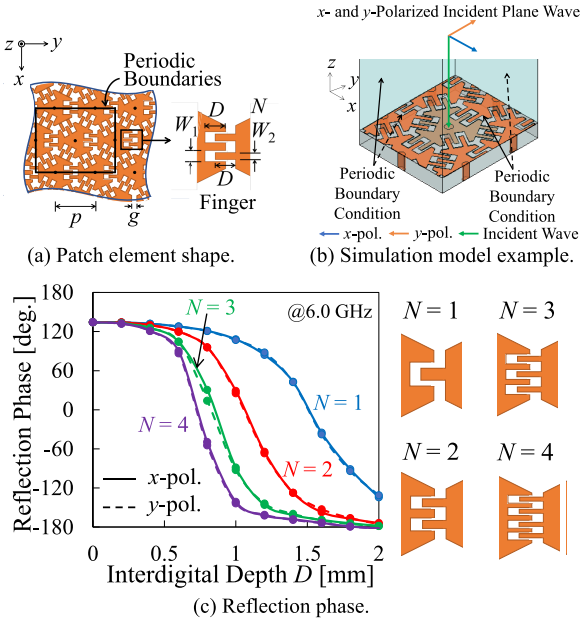

Fig. 1 Interdigital structure metasurface. (a) Patch element shape, where p is the distance (pitch) between the patch centers, D is the interdigital finger depth, N is the number of the interdigital fingers, W_1 is the finger space, and W_2 is the finger width. (b) Simulation model example, where the x- and y-polarized plane waves illuminate perpendicular to the metasurface reflector on the x-y plane and the periodic boundary conditions are set for two pair of parallel side planes, respectively. (c) Reflection phases plotted as functions of the interdigital finger depth D at the simulation frequency f_0 of 6 GHz.

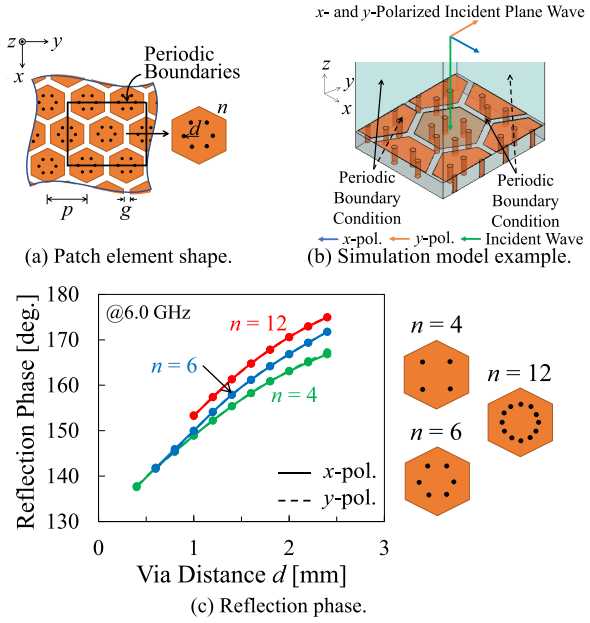

Fig. 2 Multi-via structure metasurface. (a) Patch element shape, where d is the distance from the patch center to the vias, and n is the number of vias. (b) Simulation model example, where the x- and y-polarized plane waves illuminate perpendicular to the metasurface reflector on the x-y plane and the periodic boundary conditions are set for two pair of parallel side planes, respectively. (c) Reflection phases plotted as functions of the distance d at the simulation frequency f_0 of 6 GHz.

black dots in this figure. In this paper, the convex (protruding) parts of the interdigital structures are called fingers. In Fig. 1(a), p is the distance (pitch) between the patch centers, D is the interdigital finger depth, g is the gap size between the adjacent hexagonal patches, W_1 is the finger space, and W_2 is the finger width. The finger space W_1 and the finger width W_2 should be determined to make the finger gap spaces equally. The interdigital finger number on one side of the hexagon is represented by N. Figure 1(a) shows the interdigital structure for the finger number N of 2. The capacitance of the interdigital structure could be changed by the interdigital finger depth D, so that the reflection phase of the metasurface with the interdigital structure could be designed flexibly.

Figure 1(b) shows the simulation model example, where the x- and y-polarized plane waves illuminate perpendicular to the metasurface on the x-y plane. The periodic boundary conditions are set for two pair of parallel side planes, respectively, where the periodic boundaries are also shown in Fig. 1(a). In this paper, the flame-retardant-type 4 (FR-4) substrate Panasonic R-1705 is used for the manufacturing, because this substrate is inexpensive and can be applied up to 6 GHz. According to the datasheet of this substrate, its relative permittivity ε_r of 4.7, dielectric loss tangent tan δ of 0.015, and thickness t of 1.6 mm are used for the simulations. The gap size g of 0.6 mm and the via diameter Ψ of 0.8 mm are chosen for ease of manufacturing.

The pitch p of 6 mm is small enough in comparison with the wavelength λ_0 of 50 mm corresponding to f_0. Fig. 1(c) shows the simulation results of the reflection phases corresponding to the finger number N at 6 GHz. In this figure, the solid and dashed lines show the reflection phase corresponding to the x- and y-polarized waves, respectively, where the dots represent the simulated values. Since the solid and dashed lines are almost the same, the low polarization dependency of the reflection phase could be confirmed. The finger number N of 2 is adopted for the reflector design in this paper, because the smaller reflection phase gradient is better for controlling and reproducing. In the finger number N of 2, the reflection phase range from $-174°$ to $+134°$ could be obtained by changing the depth D from 0 mm to 2 mm.

2.2 Multi-Via Structure Metasurface

The multi-via structure shown in Fig. 2(a) would be introduced for obtaining the reflection phase from $+134°$ to $+180°$, which could not be obtained in the interdigital structure. It could be qualitatively interpreted that the reflection phase of the mushroom-type metasurface would be close to the reflection phase $+180°$ of the metal conductor board by expanding the via area or increasing the number of vias. On the other hand, according to the formula in the papers [37], [38], the reflection phase of the mushroom-type metasurface reflector for the normal incident plane wave should not change corresponding to the via radius. It would be con-

sidered that this discrepancy is caused that the formula in [37], [38] was derived in the assumption of the thin vias. In the case of the large radius conductor cylinder, it is irregular in the normal printed circuit board fabrication. In this paper, instead of the large radius conductor cylinder, the multi-via structure described below would be adopted for ease of manufacturing.

In this structure, as shown in Fig. 2(a), the hexagonal patches are connected to the ground plane on the back through several vias represented by the black dots. In this figure, d is the distance from the patch center to the vias, n is the number of vias. The thickness t and other parameters of the substrate, the gap size g, and the pitch p are the same as the interdigital structure in the Sect. 2.1. The via diameter Ψ of 0.5 mm is chosen to arrange the multiple vias. Figure 2(b) shows the simulation model example, where the x- and y-polarized plane waves illuminate perpendicular to the metasurface on the x-y plane. The periodic boundary conditions are set for two pair of parallel side planes, respectively, where the periodic boundaries are also shown in Fig. 2(a). Figure 2(c) shows the reflection phases corresponding to the via number n at 6 GHz. The solid and dashed lines show the reflection phase corresponding to the x- and y-polarized incident waves, respectively, where the dots represent the simulated values. Because of the low polarization dependent properties, the solid and dashed lines are overlapped each other. The reflection phase range from +137° to +175° could be obtained by changing the via distance d and the via number n.

3. Reflector Design for Plane Wave Incident

In this section, the reflector design for the normal incident plane wave using the interdigital and multi-via integrated structures would be introduced. The simulated far field patterns of the RCS would be shown.

3.1 Metasurface Reflector Design

Figure 3 shows the proposed reflector simulation model. The x- and y-polarized plane waves illuminate perpendicular to the metasurface reflector on the x-y plane. For realizing the constant reflection angle, patch elements with the equal difference reflection phases should be arranged at equal intervals [12]–[15]. Since the incident plane is in the y-z plane, the reflection phases for each patch change gradually along the y-axis. The reflection angle α for the normal incident plane wave is given by

$$\alpha = \arcsin\left(\frac{\lambda_0 \Delta\varphi}{2\pi p}\right), \tag{1}$$

where $\Delta\varphi$ is the reflection phase difference between adjacent patch elements along the y-axis. The periodic boundary conditions shown in Fig. 3 are set for two pairs of parallel sides, respectively. For using the periodic boundary condition for the y-direction, $\Delta\varphi$ should satisfy

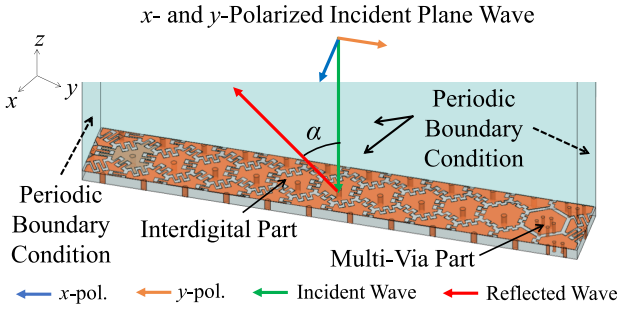

Fig. 3 Simulation model of the proposed metasurface reflector. The x- and y-polarized plane waves illuminate perpendicular to the metasurface reflector on the x-y plane.

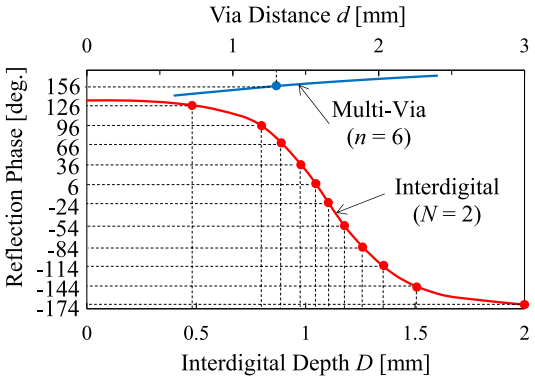

Fig. 4 Reflection phases of the selected interdigital structures with the finger depth D in the lower horizontal axis and the selected multi-via structure with the via distance d from the patch center to the vias in the upper horizontal axis, where the finger number N of 2, the via number n of 6, and the reflection phase difference $\Delta\varphi$ of 30°. The dots represent the selected values for the reflector design.

$$\Delta\varphi = \frac{2\pi}{k}, \tag{2}$$

where the integer number k is the number of patch elements along the y-axis. In Fig. 3, there are 12 patch elements ($k = 12$) with the reflection phase difference $\Delta\varphi$ of 30°. From Eq. (1), the reflection angle α should be 44° for the pitch p of 6 mm at 6 GHz. According to Fig. 1(c) and Fig. 2(c), eleven interdigital structures of the finger number N of 2 with different finger depths D and one multi-via structure of the via number n of 6 are selected to satisfy the reflection phase difference $\Delta\varphi$ of 30°. The structure decision procedure for the patch elements is described in the Sect. 3.2.

Figure 4 shows the reflection phases of the selected interdigital structures with the finger depth D in the lower horizontal axis and the selected multi-via structure with the distance d from the patch center to the vias in the upper horizontal axis, where the finger number N of 2, the via number n of 6, and the reflection phase difference $\Delta\varphi$ of 30°. The dots represent the simulated values for the reflector design. Combining the proposed two structures, the wide reflection phase range of approximately 360° could be obtained. Therefore, the reflection phases from –174° to +156° with

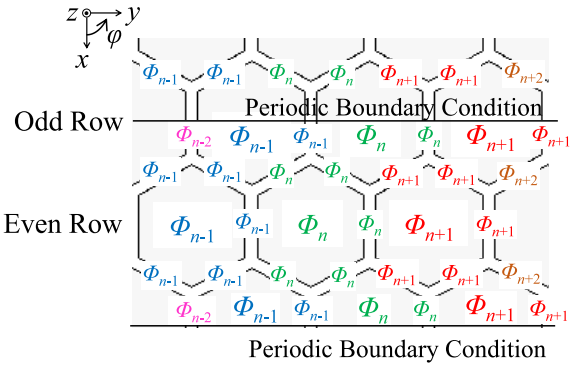

Fig. 5 Structure decision procedure for the patch elements, where the previous assigned patch reflection phase would be reassigned to the sides of the hexagonal patch under the priority of the even row and smaller number column (left side) patches.

a phase difference of 30° could be realized by composed of eleven interdigital and one multi-via structure.

3.2 Structure Decision Procedure for the Patch Elements

In the case of the hexagonal mushroom-type patches with the interdigital and multi-via structure, it is difficult to assign a reflection phase to a single patch element such as a conventional square patch reflector design. In other words, the patch element shape could not be decided from the reflection phase straightforwardly. In this paper, the structure decision procedure described below would be adopted to decide the structural parameters of the interdigital and multi-via structures. The optimization for the metasurface reflector with the proposed structures would be a future study, while the design method for achieving the high efficiency reflected beam were described in [39], [40].

The reflection phase assignment is shown in Fig. 5 corresponding to the metasurface reflector in the Sect. 3.1. In this case, the reflection phase would be varied along the y-axis. The structural parameters of the interdigital and multi-via structures would be decided as follows. First, the reflection phase Φ_n would be assigned to the hexagonal patch, where the reflection phase Φ_n satisfy

$$\Phi_{n+1} - \Phi_n = \Delta\varphi, \tag{3}$$

where n represents the column number. In spite of the y-coordinate difference of a half pitch $p/2$ for odd and even row patches, the same reflection phase Φ_n would be assigned to both odd and even row patches to minimize the phase difference along x-axis, since the reflection angle would be mainly decided by the phase difference along y-axis. Second, the previous assigned patch reflection phase Φ_n would be reassigned to the sides of the hexagonal patch under the priority of the even row and smaller number column (left side) patches, so that the reflection phase can be mainly controlled in the side structures of the hexagonal patches. Third, the finger depth D for the interdigital structure and the via distance d for the multi-via structure would be decided according to the reassigned reflection phase Φ_n, using Fig. 1(c) and Fig. 2(c).

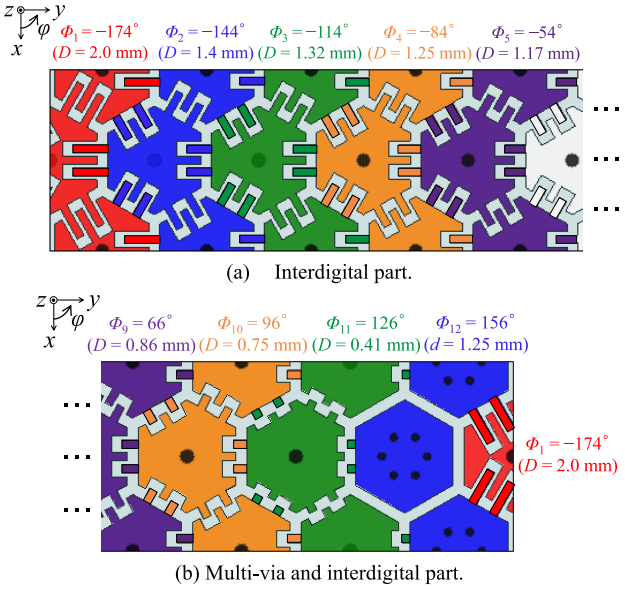

(a) Interdigital part.

(b) Multi-via and interdigital part.

Fig. 6 Interdigital and multi-via structure parts for the designed metasurface reflector with the reflection phase difference $\Delta\varphi$ of 30°, where the interdigital patches and fingers with the same reflection phase are painted in the same color. The multi-via patches with the same reflection phase are also painted in the same color.

The interdigital and multi-via structure parts for the designed metasurface reflector with the reflection phase difference $\Delta\varphi$ of 30° are shown in Fig. 6. The interdigital patches and fingers with the same reflection phase are painted in the same color. The multi-via patches with the same reflection phase are also painted in the same color.

3.3 Simulation of Metasurface Reflector

The simulated far field patterns of the RCS for the co-polarization reflected waves on the y-z plane at 6 GHz are shown in Fig. 7, where the red and blue lines show the RCS corresponding to the x- and y- polarized incident waves, respectively. The reflector size of 125 × 216 mm is used in these simulations. The sharp far field pattern and the low polarization dependent properties are observed in this figure. The maximum directivities of 3.26 dBsm and 2.97 dBsm for the x- and y-polarized incident waves are obtained at the reflection angle of 316° (−44°). The sidelobes at the direction of 0° are −7.79 dBsm and −4.55 dBsm for the x- and y-polarized incident waves, respectively, which are suppressed by 11.05 dB and 7.52 dB compared with the maximum directivities. The sidelobes at the direction of 339° (−21°) are −10.05 dBsm and −7.99 dBsm for the x- and y-polarized incident waves, respectively, which are suppressed by 13.31 dB and 10.96 dB compared with the maximum directivities. Since the cross-polarized waves are suppressed over 63.41 dB and 42.25 dB for the x- and y-polarized incident waves in comparison with the reflected wave maximum directivity, they are not shown in this figure. Therefore, when the incident plane wave is illuminated perpen-

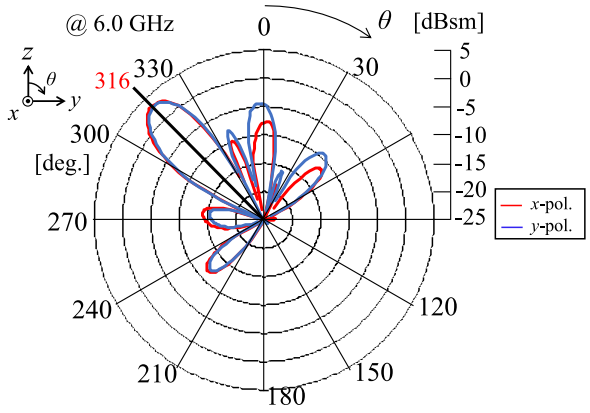

Fig. 7 Simulated far field patterns of the RCS for the co-polarized reflected waves on the *y*-*z* plane at 6 GHz, where the reflector size is 125 × 216 mm.

dicular to the reflector, the effectiveness of the interdigital and multi-via structure metasurface reflector could be confirmed.

4. Reflector Design Using the Incident Wave Phase

In this section, the design method based on the ray tracing method using the incident wave phase is described for applying the proposed structure to the arbitrary incident wave. Then, this method is applied for the prototype metasurface reflector utilized in our next stage evaluation experiments described in the Sect. 5.

4.1 Reflector Design Method Using the Incident Wave Phase

First of all, due to the size limitation of our anechoic chamber used for the evaluation experiments, the distance between the TX and the reflector could not be kept sufficiently for the far-field range. In this case, the incident wave could not be regarded as a plane wave, therefore the metasurface reflector should be designed in the same way as the primary reflector design of the reflector antenna. In this paper, the design method based on the ray tracing method using the incident wave phase is proposed. Specifically, in our proposed method, the metasurface reflector would be designed according to Pozar's method [4]. However, the incident wave phase distribution on the reflector would be obtained by the electromagnetic simulation, instead of calculating by the path length from the phase center of wave source to the reflection plane. In this case, the reflection phase distribution of the metasurface reflector would be determined using the obtained incident wave phase distribution. Then, the metasurface structures would be designed to realize this reflection phase distribution.

In this subsection, the ray tracing method [41], [42] used in the hologram optical element would be applied to the metasurface reflector design. Figure 8 shows the configuration of the ray tracing used in this paper. The reflector is placed on the *x*-*y* plane. The unit vector $(l_{out}, m_{out}, n_{out})$ of

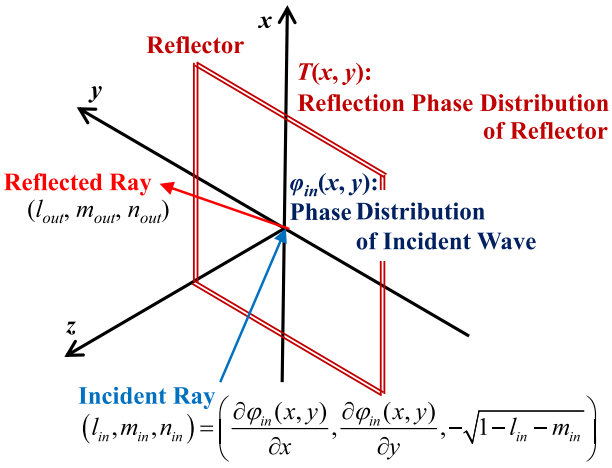

Fig. 8 Ray tracing of the reflector, where (l_{in}, m_{in}, n_{in}) is the unit vector of the incident ray, $(l_{out}, m_{out}, n_{out})$ is the unit vector of the reflected ray, $T(x, y)$ is the reflection phase distribution of the reflector, and $\varphi_{in}(x, y)$ is the phase distribution of the incident wave on the *x*-*y* plane.

the reflected ray is given by

$$l_{out} = l_{in} + \frac{\lambda_0}{2\pi}\frac{\partial\{-T(x,y)\}}{\partial x}, \tag{4a}$$

$$m_{out} = m_{in} + \frac{\lambda_0}{2\pi}\frac{\partial\{-T(x,y)\}}{\partial y}, \tag{4b}$$

$$n_{out} = \sqrt{1 - l_{out}^2 - m_{out}^2}, \tag{4c}$$

where (l_{in}, m_{in}, n_{in}) is the unit vector of the incident ray, and $T(x, y)$ is the phase transfer function of the reflector. In this paper, the phase transfer function $T(x, y)$ is called as the reflection phase distribution to apply the reflector design. Since the x and y components of the unit vector of the incident ray could be represented by the partial derivatives of the incident wave phase distribution, Eqs. (4a) and (4b) could be represented by

$$l_{out} = \frac{\lambda_0}{2\pi}\frac{\partial\{-\varphi_{in}(x,y)\}}{\partial x} + \frac{\lambda_0}{2\pi}\frac{\partial\{-T(x,y)\}}{\partial x}, \tag{5a}$$

$$m_{out} = \frac{\lambda_0}{2\pi}\frac{\partial\{-\varphi_{in}(x,y)\}}{\partial y} + \frac{\lambda_0}{2\pi}\frac{\partial\{-T(x,y)\}}{\partial y}, \tag{5b}$$

where $\varphi_{in}(x, y)$ is the incident wave phase distribution on the *x*-*y* plane. In the case that the reflected wave would be a plane wave, the components l_{out}, m_{out}, n_{out} of the reflected ray unit vector would be constants. Therefore, the reflection phase distribution $T(x, y)$ could be represented by

$$T(x,y) = -\frac{2\pi}{\lambda_0}l_{out}x - \frac{2\pi}{\lambda_0}m_{out}y - \varphi_{in}(x,y) + C + 2n\pi, \tag{6}$$

where the fourth term C as the integration constant is an arbitrary constant, n is an arbitrary integer, and the fifth term $2n\pi$ represents the phase periodicity. Since the reflection direction is determined by the gradient of the reflection phase distribution, the fourth term C does not affect the reflection direction. It could be considered that the first and second terms would determine the reflection direction and the third

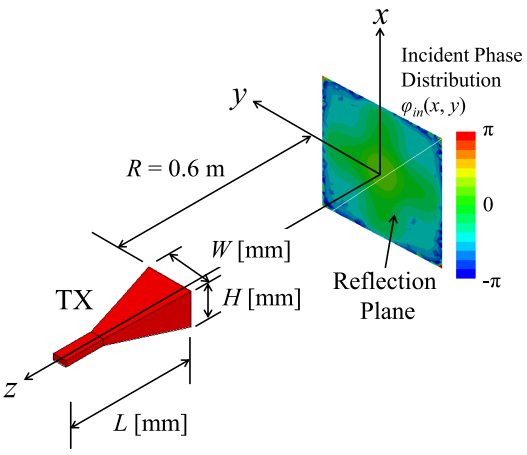

Fig. 9 Simulation model of the transmitting antenna (TX), for obtaining the incident wave phase distribution $\varphi_{\text{in}}(x, y)$ on the reflection plane.

term would compensate the incident wave phase distribution. In Eqs. (4a), (4b), (5a), and (5b), minus signs are added to $T(x, y)$ and $\varphi_{in}(x, y)$, since the opposite phase signs to the previous papers [41], [42] are used in this paper.

4.2 Reflector Design for Evaluation Experiments

Figure 9 shows the simulation model of the TX for obtaining the incident wave phase distribution $\varphi_{in}(x, y)$ on the reflection plane. The standard horn antenna ETS-Lindgren 3160-06 is used as the TX in the evaluation experiments. Its specification frequency range is from 5.85 GHz to 8.20 GHz. The aperture height H, the aperture width W, and the length L of the TX are 86 mm, 116 mm, and 305 mm, respectively. In this figure, the x-polarized wave from the TX illuminates perpendicular to the reflection plane on the x-y plane. Figure 10(a) and Fig. 10(b) show the incident wave phase examples $\varphi_{in}(x, 0)$ on the x-axis and $\varphi_{in}(0, y)$ on the y-axis, respectively, where the distance R between the antenna aperture and the reflection plane is 0.6 m for matching to our experimental setup in Sect. 5. In this figure, the solid lines show the simulated phase distribution, and the dashed lines show the phase distribution calculated by the path length from the phase center to the reflection plane for comparison. The distance between the antenna aperture and the phase center is assumed to be same as the TX length L of 305 mm. Since the simulated phase distribution is not necessary to define the accurate phase center of the wave source, it could be obtained easily and accurately in comparison with the phase distribution calculated by the path length from the phase center to the reflection plane.

The metasurface reflector with a reflection angle of 44° would be designed in this paper. Figure 11(a) and Fig. 11(b) show the calculated reflection phase distribution examples $T(x, 0)$ on the x-axis and $T(0, y)$ on the y-axis using Eq. (6), where the x-component l_{out} and the y-component m_{out} of the reflected ray unit vector are 0 and $-\sin(44°)$, respectively, the simulated incident phase distribution is used as $\varphi_{in}(x, y)$, and the constant C is determined to satisfy $T(0, 0) = 0$.

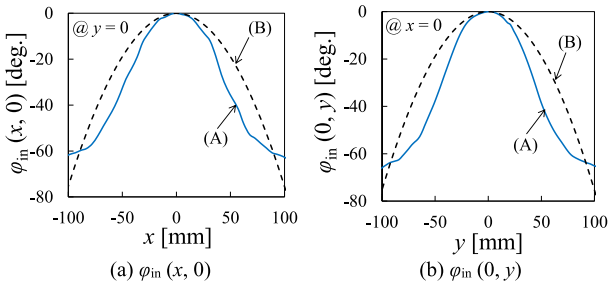

(a) $\varphi_{\text{in}}(x, 0)$ (b) $\varphi_{\text{in}}(0, y)$

Fig. 10 Incident wave phase examples. (a) $\varphi_{\text{in}}(x, 0)$ on the x-axis and (b) $\varphi_{\text{in}}(0, y)$ on the y-axis, where the solid lines show (A) the simulated phase distribution and the dashed lines show (B) the phase distribution calculated by the distance from the phase center to the reflection plane.

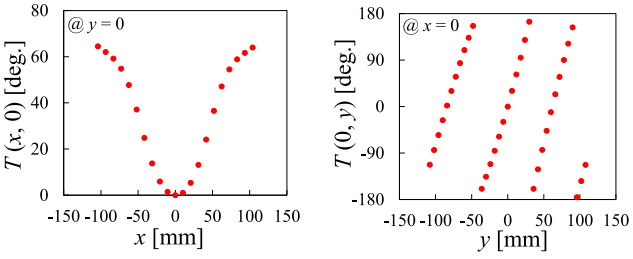

(a) $T(x, 0)$ (b) $T(0, y)$

Fig. 11 Calculated reflection phase distribution examples (a) $T(x, 0)$ on the x-axis and (b) $T(0, y)$ on the y-axis, using Eq. (6).

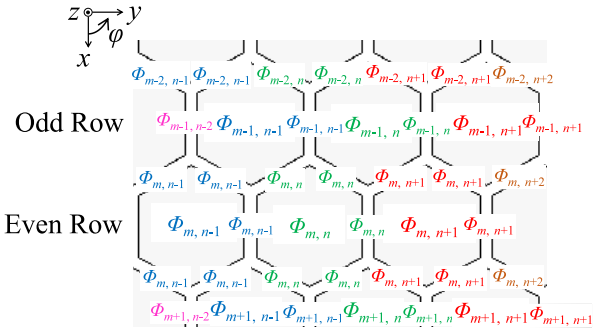

Fig. 12 Structure decision procedure for the patch elements of the proposed metasurface reflector utilized in the evaluation experiments, where the previous assigned patch reflection phase $\Phi_{m,n}$ would be reassigned to the sides of the hexagonal patch under the priority of the even row and smaller number column (left side) patches.

The reflection phase assignment shown in Fig. 12 is used as the structure decision procedure. In this procedure, similar to the Sect. 3.2, the structural parameters of the interdigital and multi-via structures would be decided as follows. First, based on the calculated reflection phase distribution $T(x, y)$, the reflection phase for the m-th row and n-th column patch $\Phi_{m,n}$ would be determined according to

$$\Phi_{2i-1,n} = -\frac{2\pi}{\lambda_0} m_{out} y_{2i,n} - \varphi_{in}\left(x_{2i-1,n}, y_{2i-1,n}\right) + C + 2n\pi, \tag{7a}$$

$$\Phi_{2i,n} = -\frac{2\pi}{\lambda_0} m_{out} y_{2i,n} - \varphi_{in}\left(x_{2i,n}, y_{2i,n}\right) + C + 2n\pi, \tag{7b}$$

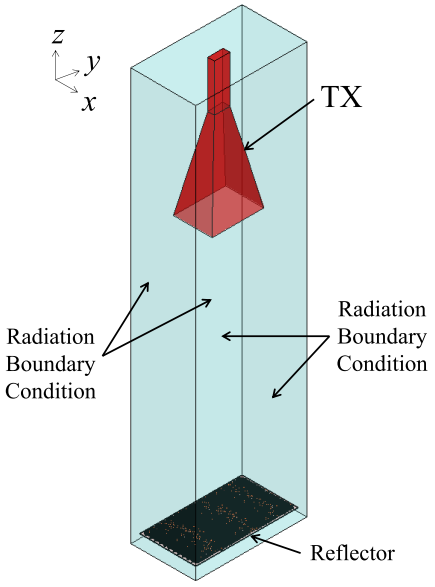

Fig. 13 Simulation model for the evaluation experiments.

where $x_{m,n}$ and $y_{m,n}$ represent the x- and y-coordinates of the m-th row and n-th column patch center, respectively and i is the integer number. Equations (7a) and (7b) represent the reflection phases for the odd row ($m = 2i - 1$) and even row ($m = 2i$) patches, respectively. Equation (7a) seems to be a little bit complicate, since the y-coordinate $y_{2i,n}$ of the even row patch is used for the odd row patch. However, to obtain the equivalent reflected wave phase to the simulation in the Sect. 3, $y_{2i,n}$ would be used for the odd row patch in Eq. (7a), as the same reflection phase is assigned to both odd and even row patches in the procedure of Sect. 3.2. Second, the previous assigned patch reflection phase $\Phi_{m,n}$ would be reassigned to the sides of the hexagonal patch under the priority of the even row and smaller number column (left side) patches same as the Sect. 3.2. Third, the finger depth D for the interdigital structure and the via distance d for the multi-via structure would be decided according to the reassigned reflection phase $\Phi_{m,n}$, using Fig. 1(c) and Fig. 2(c).

The simulation models of the reflector antenna composed of the TX and the designed reflector with the interdigital and multi-via structures are shown in Fig. 13, where the reflector size is 125×228 mm and the other parameters are the same as the Sect. 3. In this figure, the x-polarized wave from the TX would illuminate vertically the metasurface reflector on the x-y plane and the reflection pattern would be analyzed. Figure 14 shows the metasurface reflector part of the simulation model, including the expanded views. The radiation patterns of the simulation models in Figs. 13 and 14 are presented in the Sect. 5, along with measurement results.

5. Evaluation Experiments

The prototype reflectors and their evaluation experiment results are described in this section.

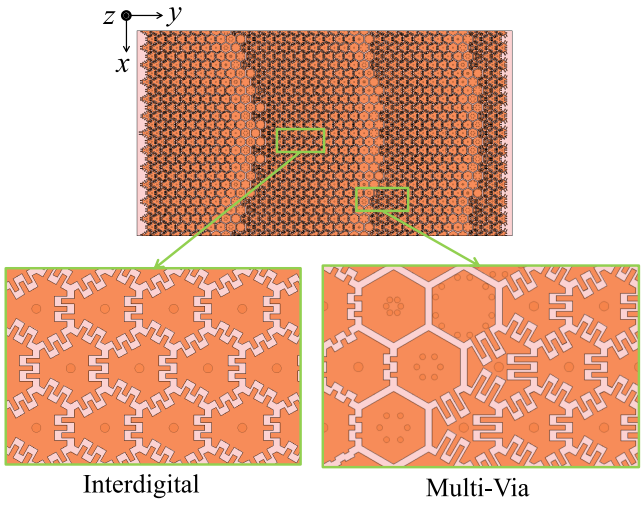

Fig. 14 Metasurface reflector part of the simulation model, including the expanded views, where the substrate size is 125×228 mm and the substrate thickness t is 1.6 mm.

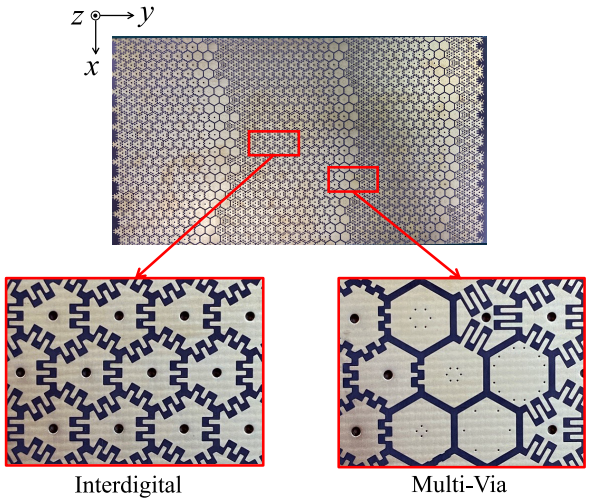

Fig. 15 Photographs of the prototype metasurface reflector with the interdigital and multi-via structures, including the expanded views, where the FR-4 substrate Panasonic R-1705 was used for the prototype. The substrate size is 125×228 mm.

5.1 Prototype Metasurface Reflector

Figure 15 shows the photographs of the prototype metasurface reflector with the interdigital and multi-via structures, including the expanded views, where the substrate size is 125×228 mm as same as the simulation model in the Sect. 4. Using the structure data provided from the simulator, the prototype metasurface reflectors were manufactured by a printed circuit board manufacturer. The FR-4 substrate Panasonic R-1705 was used for the manufacture, as described in the Sect. 2.1.

5.2 Reflector Measurement System

For the evaluation experiments of the reflectors, the mea-

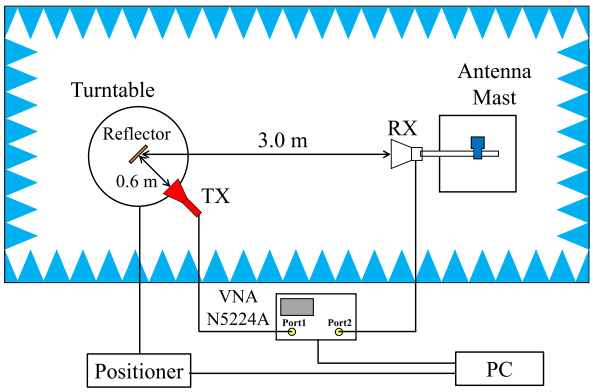

Fig. 16 Measurement system for the reflector, including the TX and the receiving antenna (RX). The vector network analyzer (VNA) and the turntable could be controlled by the personal computer (PC). The positioner is the control unit for the turntable.

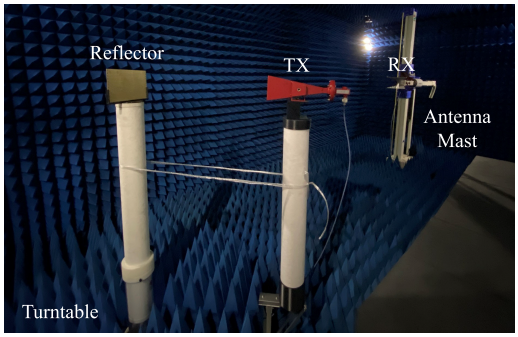

Fig. 17 Inside photograph of the anechoic chamber with the measurement equipment, including the TX and the RX.

surement system shown in Fig. 16 is set up in our anechoic chamber. Figure 17 shows the inside photograph of our anechoic chamber with the equipment of the measurement system, including the standard horn antenna ETS-Lindgren 3160-06 for the TX and the wideband antenna ETS-Lindgren 3115 for the receiving antenna (RX). The reflector is placed on the top of a styrofoam pole in the center of the turntable which is usually used in the electromagnetic compatibility (EMC) measurement. The TX is placed on the top of another styrofoam pole in the edge of the turntable. The distance from the TX aperture to the reflector is 0.6 m, which is same as the radius of the turntable. The RX is held at the antenna mast on the floor outside the turntable. The distance from the reflector to the RX aperture is 3 m because of the limitation of our anechoic chamber. The reflector, the TX, and the RX are placed at the same height of 1.45 m from the floor, which is the height center of chamber. By rotating the turntable with maintaining the relative position of the TX and the reflector, the reflection pattern on the horizontal plane could be measured by the RX, where the vector network analyzer (VNA) Keysight N5224A was used for this measurement. The VNA and the turntable could be controlled by the personal computer (PC).

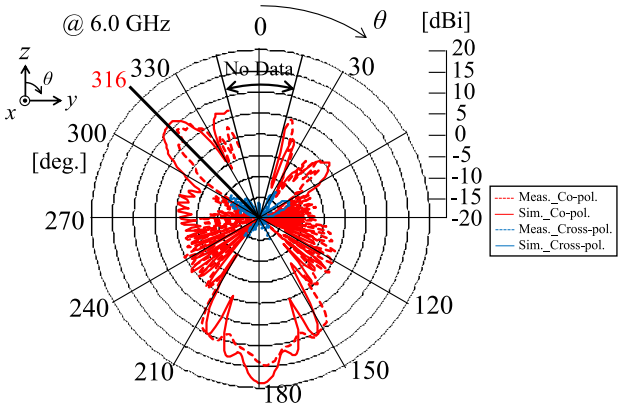

Fig. 18 The radiation patterns in the actual gain for the reflector antenna composed of the transmitting horn antenna and the prototype metasurface reflector. The dotted and solid lines show the measurement and simulation results, respectively.

5.3 Measurement Results

Figure 18 shows the radiation patterns in the actual gain for the reflector antenna composed of the TX and the prototype metasurface reflector. In this figure, the dotted and solid lines show the measurement results and the simulation results, respectively. The red and blue lines show the co- and cross-polarized components, respectively. In Fig. 18, the measured values are calibrated with 15.9 dBi, which is the authorized actual gain of the standard horn antenna ETS-Lindgren 3160-06. Because the TX would scatter the reflected wave from the reflector to the RX in our simulation model and measurement system of Figs. 13 and 16, the measured and simulated radiation patterns around at the angle of 0° could not show true radiation patterns. Therefore, the radiation patters at the angle range from 345° (−15°) to 15° are omitted in Fig. 18, referring to some manuscripts [8], [13], [14]. The maximum directivities for the measured and simulated results are obtained at the reflection direction of 318° (−42°) and 317° (−43°), respectively, which are similar to the designed reflection angle of 316° (−44°). The effectiveness of the proposed structure and design method could be confirmed by matching the experiment and simulation results. It could be considered that the difference 2.24 dB between the measured maximum value of 8.86 dBi and the simulated maximum value of 11.1 dBi would be mainly caused by the misalignment in the measurement. The cross-polarized waves are suppressed over 19.7 dB and 23.3 dB for the measured and simulated results, respectively, in comparison with the co-polarized maximum values. However, the measured first sidelobe level at the direction of 18° and the simulated first sidelobe level at the direction of 337° (−23°) are 4.4 dBi and 6.91 dBi, respectively, which are only suppressed by 4.46 dB and 4.19 dB compared with the measured and simulated maximum directivities. The measured and simulated backlobe levels at the direction of 180° are 14.5 dBi and 19.0 dBi, respectively, which are larger than the measured and simulated main lobe

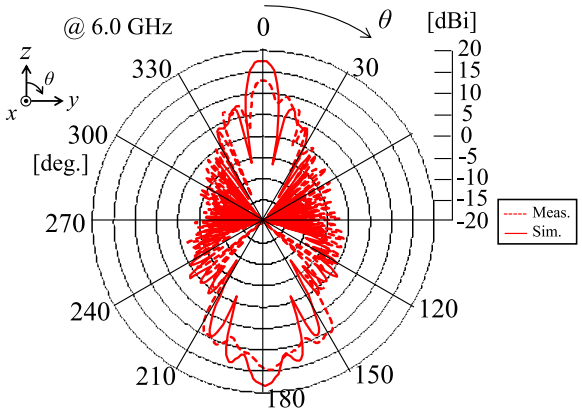

Fig. 19 The radiation patterns in the actual gain for the metal reflector antenna composed of the transmitting horn antenna and the metal reflector. The dotted and solid lines show the measurement and simulation results, respectively.

levels. To describe these reasons, Fig. 19 shows the radiation patterns in the actual gain for the planar metal reflector antenna composed of the TX and the metal reflector with the same size as the prototype metasurface reflector. In this figure, the dotted and solid lines show the measurement results and the simulation results, respectively. As described above, the TX might scatter the reflected wave in our measurement system. In Fig. 19, the large sidelobes of the metal reflector at the direction of 340° (−20°) and 20°, which should not be large [43], are confirmed in this measurement system. Especially, the measured sidelobe level of the metal reflector antenna at the direction of 17° is 7.5 dBi, which is only suppressed by 5.56 dB compared with the measured maximum directivities of 13.06 dBi. Therefore, it would be considered that the large sidelobes at the angle of 340° (−20°) and 20° of the prototype metasurface reflector antenna are also caused by the measurement system. In addition, due to the limitation of our existing computer specifications etc., the relatively small prototype reflector was used for experiments, though the small reflector has large backlobe. As shown in Figs. 18 and 19, since the backlobe patterns of the metasurface and metal reflector antennas are approximately same, it could be considered that the large backlobes are caused by the small size of reflector. Improving the sidelobe and backlobe levels would be a future study.

6. Conclusion

Novel patch element shapes with the interdigital and multi-via structures for hexagonal patch mushroom-type metasurface reflectors were proposed for obtaining the reflection phase range of ±180°. These proposed structures could be realized inexpensively using the usual double-sided print circuit board fabrication. Using these structures, the reflection phase range from −174° to +175° could be confirmed in the electromagnetic field simulation. A design method of the proposed reflector with the novel structures was introduced. The metasurface reflector with a reflection angle of 44° for the normal incident plane wave was designed and simulated. The simulated maximum directivities were the same as the designed reflection angle. The low polarization dependent properties and the sharp far field patterns were confirmed in the simulation results. The prototype metasurface reflector with its size of 125 × 228 mm was designed and manufactured for the evaluation experiments. Due to the size limitation of our anechoic chamber, the prototype reflector should be designed in the same way as the primary reflector design of the reflector antenna. Specifically, the reflector design method based on the ray tracing method using the incident wave phase was proposed, for applying the proposed structure to the arbitrary incident wave. The measured radiation pattern for the reflector antenna composed of the TX and the prototype metasurface reflector was similar to the simulated radiation pattern. The effectiveness of the proposed structures and the design method could be confirmed by these simulation and experiment results. In order to improve the sidelobe and backlobe levels, the optimization for the metasurface reflector with the proposed structures would be a future study.

Acknowledgments

The authors would like to thank Prof. Michishita of the National Defense Academy and Dr. Matsuno of the KDDI Research, Inc. for their kind support. This research was partly supported by JSPS KAKENHI Grant Number C21K04050.

References

[1] T.S. Rappaport, S. Sun, R. Mayzus, H. Zhao, Y. Azar, K. Wang, G.N. Wong, J.K. Schulz, M. Samimi, and F. Gutierrez, "Millimeter wave mobile communications for 5G cellular: It will work!," IEEE Access, vol.1, pp.335–349, May 2013.

[2] W. Khawaja, O. Ozdemir, Y. Yapici, F. Erden, and I. Guvenc, "Coverage enhancement for NLOS mmWave links using passive reflectors," IEEE Open J. Commun. Soc., vol.1, pp.263–281, Jan. 2020.

[3] Z. Peng, L. Li, M. Wang, Z. Zhang, Q. Liu, Y. Liu, and R. Liu, "An effective coverage scheme with passive-reflectors for urban millimeter-wave communication," IEEE Antennas Wireless Propag. Lett., vol.15, pp.398–401, June 2015.

[4] D.M. Pozar, T.S. Targonsky, and H.D. Syrigos, "Design of millimeter wave microstrip reflectarrays," IEEE Trans. Antennas Propag., vol.45, no.2, pp.287–296, Feb. 1997.

[5] L. Li, Q. Chen, Q. Yuan, K. Sawaya, T. Maruyama, T. Furuno, and S. Uebayashi, "Frequency selective reflectarray using crossed-dipole elements with square loops for wireless communication applications," IEEE Trans. Antennas Propag., vol.59, no.1, pp.89–99, Jan. 2011.

[6] L. Li, Q. Chen, Q. Yuan, K. Sawaya, T. Maruyama, T. Furuno, and S. Uebayashi, "Novel broadband planar reflectarray with parastic dipoles for wireless communication applications," IEEE Antennas Wireless Propag. Lett., vol.8, pp.881–885, July 2009.

[7] T. Maruyama, T. Furuno, T. Ohya, Y. Oda, Q. Chen, and K. Sawaya, "Dual frequency selective reflectarray for propagation improvement," Proc. Int. Workshop on Antenna Technol., Lisbon, Portgal, March 2010.

[8] J.F. Li, Q. Chen, Q.W. Yuan, and K. Sawaya, "Reflectarray element using interdigital gap loading structure," Electron. Lett., vol.47, no.2, pp.83–85, Jan. 2011.

[9] J.F. Li, Q. Chen, K. Sawaya, and Q.W. Yuan, "Inverted-L reflectarray element with interdigital gap loading structure," Proc. 2012 IEEE Int. Symp. on Antennas Propag., pp.1389–1392, Nagoya, Japan, Nov. 2012.
[10] Q.Y. Chen, S.W. Qu, J.F. Li, Q. Chen, and M.Y. Xia, "An X-band reflectarray with novel elements and enhanced bandwidth," IEEE Antennas Wireless Propag. Lett., vol.12, pp.317–320, March 2013.
[11] T. Murayama, S. Sasaki, D. Higashi, H. Deguchi, and M. Tsuji, "Reflectarray antenna constructed by arranging double omega-shaped resonant elements for orthogonal-polarization conversion," Proc. 2018 IEEE Int. Symp. on Antennas Propag., Busan, Korea, Oct. 2018.
[12] K. Chang, J. Ahn, and Y.J. Yoon, "Artificial surface having frequency dependent reflection angle," Proc. 2008 IEEE Int. Symp. on Antennas Propag., Taipei, Taiwan, Jan. 2008.
[13] T. Maruyama, T. Furuno, and S. Uebayashi, "Experiment and analysis of reflect beam direction control using a reflector having periodic tapered mushroom-like structure," Proc. 2008 IEEE Int. Symp. on Antennas Propag., Taipei, Taiwan, Jan. 2008.
[14] T. Maruyama, T. Furuno, Y. Oda, J. Shen, and T. Ohya, "Capacitance value control for metamaterial reflectarray using multi-layer mushroom structure with parasitic patches," ACES J., vol.27, no.1, pp.28–41, Jan. 2012.
[15] T. Maruyama, T. Furuno, Y. Oda, J. Shen, N. Tran, and H. Kayama, "Design of wide angle reflection reflectarray using multi-layer mushroom structure to improve propagation," Proc. 30th URSI General Assembly and Scientific Symp., Istanbul, Turkey, pp.1–4, Aug. 2011.
[16] T. Maruyama, J. Shen, N. Tran, and Y. Oda, "Novel H-type mushroom-like structure for multi-band reflectarray," Proc. 2013 IEEE-APS Topical Conf. on Antennas and Propag. in Wireless Commun., Turin, Italy, Sept. 2013.
[17] T. Maruyama, T. Shimano, Q. Chen, S. Kameda, and N. Suematsu, "Novel reflected beam switching method using meta-surface loaded with active elements," Proc. 2017 IEEE-APS Topical Conf. on Antennas and Propag. in Wireless Commun., Verona, Italy, Sept. 2017.
[18] R. Kuse, T. Hori, and M. Fujimoto, "Variable-reflection-angle metasurface using double-layered patch-type FSS," IEICE Commun. Express, vol.5, no.8, pp.290–296, June 2016.
[19] T. Hongnara, Y. Shirasawa, T. Sasaki, K. Sasaki, K. Sato, I. Oshima, N. Michishita, H. Nakabayashi, and K. Cho, "Dual-polarized broadbeam reflective metasurface based on multi-sheet configuration for local 5G application at 28.25 GHz," Proc. 15th Eur. Conf. on Antennas Propag, Dusseldorf, Germany, March 2021.
[20] T. Maruyama, S. Endo, Q. Chen, S. Kameda, and N. Suematsu, "Reflectarray design for small antenna using meta-surface," Proc. 2016 IEEE-APS Topical Conf. on Antennas and Propag. in Wireless Commun., Cairns, QLD, Australia, pp.250–251, Sept. 2016.
[21] Y. Ishii, T. Masaki, N. Michishita, H. Morishita, and H. Hada, "Experimental consideration of RCS reduction using thin metasurface," IEICE Commun. Express, vol.6, no.6, pp.249–253, Feb. 2017.
[22] Y. Kawakami, R. Kuse, and T. Hori, "Decoupling of dipole antenna array on patch type meta-surface with C-shaped parasitic element," Proc. 13th Eur. Conf. on Antennas Propag, Krakow, Poland, March 2019.
[23] D. Sievenpiper, L. Zhang, R.F.J. Broas, N.G. Alexopolous, and E. Yablonovitch, "High-impedance electromagnetic surfaces with a forbidden frequency band," IEEE Trans. Microw. Theory Techn., vol.47, no.11, pp.2059–2074, Nov. 1999.
[24] D.F. Sievenpiper, "High-impedance electromagnetic surface," Ph.D. Dissertation, UCLA, 1999.
[25] K. Zhang, A. Zhang, and S. Yan, "A compact antenna based on metasurface for WLAN band," Proc. 2019 IEEE Int. Symp. on Antennas Propag., Xi'an, China, Jan. 2020.
[26] C. Hsu, N. Liu, S. Wu, and J. Tarng, "An ultra-wideband millimeter wave aperture-coupled patch antenna using a comb-shaped metasurface," Proc. 2019 Asia Pacific Microw. Conf., Singapore, pp.658–660, Dec. 2019.
[27] T. Yue, Z. Jiang, and D.H. Werner, "Compact, wideband antennas enabled by interdigitated capacitor-loaded metasurfaces," IEEE Trans. Antennas Propag., vol.64, no.5, pp.1595–1606, May 2016.
[28] C. Caloz and T. Itoh, Electromagnetic Metamaterials: Transmission Line Theory and Microwave Applications, pp.170–173, Wiley, New Jersey, 2006.
[29] A. Presse, X. Zhang, M. Mantash, A.C. Tarot, and J.M. Floch, "Miniaturization of an artificial magnetic conductor with interdigital capacitances," Proc. 2015 Loughborough Antennas Propag. Conf., Loughborough, UK, Nov. 2015.
[30] R. Saad and K.L. Ford, "A miniaturised dual band artificial magnetic conductor using interdigital capacitance," Proc. 8th Eur. Conf. on Antennas Propag, the Hague, the Netherlands, pp.25–26, April 2014.
[31] X. Liu and G. Lu, "A novel broadband EBG using multi-via and double-layer structure," Proc. 2016 Progress In Electromagnetic Research Symposium, Shanghai, China, Aug. 2016.
[32] Y. Zhang, W. Zhang, T. Hong, S. Lü, and X. Ni, "Stop-band analysis of multi-via EBG structure," Proc. 2012 Int. Conf. Microw. Millim. Wave Technol., Chengdu, China, May 2012.
[33] W. Zhang, C. Liang, T. Ding, and B. Wu, "A novel broadband EBG using multi-via cascaded mushroom-like structure," Proc. 2009 Asia Pacific Microw. Conf., Singapore, pp.484–487, Dec. 2009.
[34] F. Yang and Y. Rahmat-Samii, "Polarization dependent electromagnetic band gap (PDEBG) structure: Design and applications," Microwave Opt. Technol. Lett., vol.41, no.6, pp.439–444, July 2004.
[35] L. Liu, F. Yang, S. Xu, and M. Li, "A high gain dual-polarization reflectarray antenna design using modified mushroom elements," Proc. 2021 IEEE Asia Pacific Microw. Conf., Brisbane, Australia, pp.34–36, Dec. 2021.
[36] T. Urakami, T. Maruyama, and T. Shiozawa, "Interdigital and multi-via structures for mushroom-type metasurface reflectors," Proc. 2020 IEEE Int. Symp. on Antennas Propag., Osaka, Japan, Jan. 2021.
[37] O. Luukkonen, C.R. Simovski, A.V. Raisanen, and S.A. Tretyakov, "An efficient and simple analytical model for analysis of propagation properties in impedance waveguides," IEEE Trans. Microw. Theory Techn., vol.56, no.7, pp.1624–1632, July 2008.
[38] O. Luukkonen, F. Costa, C.R. Simovski, A. Monorchio, and S.A. Tretyakov, "A thin electromagnetic absorber for wide incidence angles and both polarizations," IEEE Trans. Antennas Propag., vol.57, no.10, pp.3119–3125, Oct. 2009.
[39] A. Díaz-Rubio, V.S. Asadchy, A. Elsakka, and S.A. Tretyakov, "From the generalized reflection law to the realization of perfect anomalous reflectors," Sci. Adv., vol.3, no.8, e1602714, pp.1–10, Aug. 2017.
[40] Y. Kato, K. Omori, and A. Sanada, "D-band perfect anomalous reflectors for 6G applications," IEEE Access, vol.9, pp.157512–157521, April 2021.
[41] K.A. Winick and J.R. Fienup, "Optimum holographic elements recorded with nonspherical wave fronts," J. Opt. Soc. Am., vol.73, no.2, pp.208–217, Feb. 1983.
[42] J.N. Latta, "Computer-based analysis of holography using ray tracing," Appl. Opt., vol.10, no.12, pp.2698–2710, Dec. 1971.
[43] R. Ross, "Radar cross section of rectangular flat plates as a function of aspect angle," IEEE Trans. Antennas Propag., vol.14, no.3, pp.329–335, May 1966.

Taisei Urakami received the B.S. degree from National Institute of Technology (KOSEN), Kagawa College, Kagawa, Japan in 2022, and the M.S. degree from Nara Institute of Science and Technology (NAIST), Nara, Japan in 2023. He is currently a Ph.D. student with the NAIST, Nara, Japan. He is a student member of IEICE. His research interests include metasurface reflector, deep learning-based beam training for intelligent reflecting surface-assisted mmWave systems, and microwave circuits.

Tamami Maruyama received her B.S. and M.S. degrees in 1985 and 1988, respectively, from the department of mathematics, Tsuda University, Tokyo, Japan. In 2001, she received her Ph.D. degree from Tohoku University, Sendai, Japan. In 1988, she joined the Nippon Telegraph and Telephone Corporation (NTT). In 2003, she joined NTT DOCOMO INC. In 2014, she joined National Institute of Technology, Hakodate College as professor. In 1995, she received the Young Engineer Award from IEEE AP-S Tokyo Chapter. In 1998, she received the Excellent Paper Award from the IEICE. In 2008, she received the Best Paper Award from ISAP 2008. Prof. Maruyama is a member of the IEEE and IEICE. Her main research interests include the application of the meta-surface, metamaterials and reflectarray to wireless communications, wireless power transmission, optimum antenna design method, and genetic algorithm.

Shimpei Nishiyama is currently with advanced course of National Institute of Technology (KOSEN), Kagawa College, Kagawa, Japan in 2023. He is a student member of IEICE. His research interests include metasurface reflector.

Manato Kusamizu is currently with advanced course of National Institute of Technology (KOSEN), Kagawa College, Kagawa, Japan in 2022. He is a student member of IEICE. His research interests include metasurface reflector.

Akira Ono received the B.E. and M.E. degrees from the University of Electro-Communications, Japan in 1994 and 1996 respectively. He received Ph.D. degree from Tokushima Univ. in 2010. He has worked in National Institute of Technology, Kagawa College, Japan, since 1996. He is currently a professor. His research interest includes metasurface reflector.

Takahiro Shiozawa received his B.S. degree in electrical engineering from the Tokyo University of Agriculture and Technology, Tokyo, Japan, in 1980, and his M.S. degree and Ph.D. degree in electrical engineering from the University of Tokyo, Tokyo, Japan, in 1982 and 2005, respectively. In 1982, he joined the Yokogawa Electric Corporation, Tokyo, Japan. From 1987 to 1988, he was with the Optical Measurement Technology Development Company, Ltd., Tokyo, Japan. In 1990, he joined the NEC Corporation, Kanagawa, Japan. In 2007, he joined the National Institute of Technology (KOSEN), Kagawa College, Kagawa, Japan. He is currently with the Toyo University, Saitama, Japan. His research interests include metamaterials, microwave photonics, optical electronics and optical communication systems. Dr. Shiozawa is a member of the Institute of Electronics, Information, and the Institute of Image Information and Television Engineers.